ORIGINAL ARTICLE

Electrical, magnetic, and corrosion resistance properties of TiO$_2$ nanotubes filled with NiFe$_2$O$_4$ quantum dots and Ni–Fe nanoalloy

Mohamed Bahgat · Ahmed A. Farghali ·
Ahmed F. Moustafa · Mohamed H. Khedr ·
Mohassab Y. Mohassab-Ahmed

Abstract This work was carried out as an integral part of a project aiming to improve the catalytic, electrical, magnetic, and mechanical properties of synthesized TiO$_2$NTs filled with metal ferrites. TiO$_2$ nanotubes in the anatase-phase (TiO$_2$NTs) were prepared using a hydrothermal method followed by ion exchange and phase transformation. The obtained TiO$_2$NTs were filled with NiFe$_2$O$_4$ quantum dots (QDs) and then reacted at 600 °C in a reducing atmosphere to produce TiO$_2$NTs filled with Ni–Fe nanoalloy. The effect of the TiO$_2$NTs' coating on the dissolution rate of Ni–Fe nanoalloy in 0.5 M HCl solution was monitored chemically using a weight-loss technique that was performed at different temperatures. The TiO$_2$NTs' coating exhibited high protective performance and amazing corrosion resistance. The magnetic properties of the TiO$_2$NTs filled with NiFe$_2$O$_4$ QDs and Ni–Fe nanoalloy compacts were analyzed by a vibrating sample magnetometer. The electrical conductivity-temperature dependence of anatase TiO$_2$NTs, anatase TiO$_2$NTs filled with NiFe$_2$O$_4$ quantum dots, anatase TiO$_2$NTs filled with Ni–Fe nanoalloy, and NiFe$_2$O$_4$ was measured in the temperature range of 25–850 °C. The conductivity increased with temperature, indicating the semiconductor-like nature of the sample. During cooling, the conductivity retains values higher than that obtained during heating.

Introduction

TiO$_2$ is frequently used as protective coatings (Meinert et al. 1998). This is due to photo-induced charge transfer processes that occur at the semiconductor interface. TiO$_2$ coatings have been investigated for potential applications in a wide variety of fields such as solar cells and pollutant degradation (Shen et al. 2005). Recently, the applications of the TiO$_2$ coatings for cathodic protection of metals under ultraviolet (UV) illumination were reported (Park et al. 2001; Ohko et al. 2001; Yuan and Tsujikawa 1995). When a metal coated with a thin TiO$_2$ coating is exposed to UV irradiation, electron–hole pairs are generated in the TiO$_2$ coating. The photogenerated electrons can be transferred to the metal substrate thereby making its electrode potential more negative than its corrosion potential. Furthermore, titania does not get consumed because the anodic reaction is not the decomposition of TiO$_2$ itself but the oxidation of water and/or adsorbed organic species by the photogenerated holes, unlike a sacrificial-type cathode protection (Li et al. 2005; Subasri et al. 2006). Titania has been used to reinforce metallic coatings improving wear resistance, hardness, corrosion resistance and other properties (Deguchi et al. 2001; Shiyan et al. 2010; Radhakrishnana et al. 2009; Li et al. 2002; Sang et al. 2005). It was reported that the incorporation of TiO$_2$ in zinc coatings

M. Bahgat
Pyrometallurgy Laboratory, Minerals Technology Department,
Central Metallurgical Research and Development Institute
(CMRDI), Helwan, Cairo, Egypt

A. A. Farghali · A. F. Moustafa · M. H. Khedr
Nanoscience and Nanotechnology Unit,
Chemistry Department, Faculty of Science,
Beni-Sueif University, Beni-Sueif 62111, Egypt

M. Y. Mohassab-Ahmed (✉)
Metallurgical Engineering Department, University of Utah,
Salt Lake City, UT 84112, USA
e-mail: mohassab.yousef@utah.edu

led to the improvement in crystal size, enhanced corrosion resistance and microhardness, making TiO_2Zn composite coatings better compared to the pure zinc coatings (Praveen and Venkatesha 2008). The corrosion resistance enhancement is due to physical barriers created by TiO_2; TiO_2-fills crevices, gaps and micron holes on the surface of the zinc coating. However, pure TiO_2 could not be used under dark conditions, because of the charge recombination problem (Shen et al. 2005). It was reported that a Fe doped TiO_2 layer under the TiO_2 coating could retard the potential ennoblement (Shinohara 2001). It was also expected that the TiO_2 coatings modified by anions could be used as excellent protective coatings for metals in various applications (Hong et al. 2007). N-modified TiO_2, Cl-modified TiO_2 and S-modified TiO_2 coated on 316L stainless steel prepared by a sol–gel and dip-coating techniques were examined for corrosion protection of that 316L steel. It was found that the N-modified TiO_2 coating showed a remarkable improvement in corrosion protection of 316L stainless steel in 0.5 M NaCl. The charge recombination problem could also be overcome by coupling another semiconductor that has a different energy level, which could reduce charge recombination in addition to charge build-up during illumination (Tatsuma et al. 2001, 2002; Vinodgopal et al. 1996; Zhaoyue et al. 2003; Subasri and Shinohara 2003). These charges could subsequently be released in the dark, thus maintaining a more negative potential, creating cathodic protection. Based on this principle, both WO_3 (Tatsuma et al. 2001, 2002) and SnO_2 (Vinodgopal et al. 1996; Zhaoyue et al. 2003; Subasri and Shinohara 2003) have been successfully coupled with TiO_2.

It was reported that the magnetic properties of a $MnFe_2O_3$–TiO_2 composite were measured within a magnetic field of 10 kOe at room temperature and exhibited super-paramagnetic behavior resulting from $MnFe_2O_4$ nanoparticles (Peng et al. 2005; Xiao et al. 2006). In addition, the anatase TiO_2-coated $NiFe_2O_4$ nanoparticles retained the characteristics of uncoated nanocrystalline nickel ferrites, super-paramagnetism (absence of hysteresis, remanence and coercivity at 300 K), non-saturation of magnetic moments at high field (Rana et al. 2005). The magnetic measurements showed that anatase TiO_2-coated $NiFe_2O_4$ nanoparticles had lower magnetization compared to uncoated $NiFe_2O_4$ nanoparticles because of the volume contribution of the non-magnetic coating layer to the total sample volume. This could be explained by the interparticle dipole–dipole interactions within the magnetic particle volume fraction in the composite nanoparticles (Lunhong and Jing 2009). The retention of magnetic strength indicated that the movement of the composite nanoparticles could be controlled by a magnetic field, facilitating their application as removable anti-microbial

photocatalytic nanoparticles. Furthermore, it was found that $TiO_2/SiO_2/NiFe_2O_4$ magnetic composite particles could be recovered by applying an external magnetic field, and could enhance the separation efficiency for treating water (Jin et al. 2010).

On the other hand, the conductivity in TiO_2 nanocrystals depends on defects within the crystal lattice and the oxygen vacancies (Millot et al. 1987). The defects may be point defect, oxygen vacancies or Ti interstitials, or two-dimensional planer defects known as crystallographic shear planes (CSP) (Sorensen, 1981). It was reported that $Sr_3Fe_2O_{6+\delta}$ and titania-doped derivatives $Sr_3Fe_{2-x}Ti_xO_{6+\delta}$ were mixed ion–electron conductors with an energy gap of 2.3 eV (Zainullina et al. 2006). In addition, the electrical conduction in ferrites, which was a combination of electronic and ionic conduction, is dominated by electrons at low temperatures, whereas at high temperature, it was dominated by the ionic hopping mechanism (Seshamma et al. 2006).

In this paper, TiO_2NTs were used as corrosion-protection coating materials for Ni–Fe nanoalloys. The corrosion resistant performance of TiO_2NTs was measured in 0.5 M HCl solution over different immersion times and at different reaction temperatures via weight-loss measurements. The changes in the magnetic and electrical conductivity properties from filling the TiO_2NTs with $NiFe_2O_4$ QDs and Ni–Fe nanoalloy were also investigated.

Experimental

To prepare anatase-phase TiO_2NTs, 5 g of TiO_2 powder was dispersed in 150 mL of 10 M NaOH and stirred for 15 min. The dispersion was then transferred to a Teflon-lined autoclave kept at 150 °C for 144 h. A white precipitate ($Na_2Ti_3O_7$) was obtained. This precipitate was washed with HCl to neutralize the excess NaOH and to replace Na^+ to form $H_2Ti_3O_7$ nanosheets through ion-exchange process. Anatase-phase TiO_2NTs could then be obtained by heat treatment dehydration process at 500 °C.

To fill TiO_2NTs with $NiFe_2O_4$, an aqueous solution of $Ni(NO_3)_2$ and $Fe(NO_3)_3$ with molar ratio of 1:2 was mixed with TiO_2NTs and stirred with a magnetic stirrer for 30 min under vacuum. The mixture was then kept overnight, filtered and washed with distilled water. The precipitate was transferred to a beaker containing 50 mL of 1 M NaOH and stirred for 30 min at 60 °C, filtered, washed well with distilled water, dried at 100 °C for 1 h and finally fired at 600 °C for 3 h to form $NiFe_2O_4$–TiO_2NTs.

$NiFe_2O_4$ was prepared by the self-flash combustion method described in detail elsewhere (Farghali et al. 2008, 2012). In this method, an aqueous solution of $Ni(NO_3)_2$ and

Fe(NO$_3$)$_3$ with molar ratio of 1:2 was dried at 100 °C for 24 h. Then the resulting powder was heated vigorously on hot plate to ensure the complete decomposition of nitrates. Finally the obtained powder was heated at 600 °C for 3 h to form NiFe$_2$O$_4$ with crystal size ranging from 9 to 12 nm (Farghali et al. 2012).

Ni–Fe nanoalloy was prepared by the reduction of the synthesized NiFe$_2$O$_4$ under H$_2$ flow at 600 °C to produce Ni–Fe nanoalloy with particle size in the range of 8–10 nm (Bahgat et al. 2007; Lee et al. 1997). The same procedure was adopted to prepare TiO$_2$NTs filled with Ni–Fe nanoalloy where NiFe$_2$O$_4$–TiO$_2$NTs was reduced with H$_2$ at 600 °C to produce Ni–Fe with similar particle size to that of the free nanoalloy. The complete reduction of NiFe$_2$O$_4$ and the formation of Ni–Fe nanoalloy were confirmed by XRD and TEM (Fathi 2011). The samples were analyzed by transmission electron microscope (TEM-JOEL, JEM-1234), X-ray diffractometer (JSX-60P JEOL). Figure 1 shows TEM images of empty anatase TiO$_2$, anatase TiO$_2$NTs filled with NiFe$_2$O$_4$ QDs, anatase TiO$_2$NTs filled with Ni–Fe nanoalloy, and NiFe$_2$O$_4$.

Corrosion resistance measurements

Equal weights of free Ni–Fe nanoalloy and Ni–Fe nanoalloy coated with TiO$_2$NTs were compressed into disks using a cylindrical mould of 1-cm inner diameter using an applying pressure 250 kg/m^2. The disks were then heated at 110 °C for about 2 h and weighed before immersion in 0.5 M HCl solution for 20, 40, 60 and 150 min at different temperatures ranged from 25 to 75 °C. The corrosion rate was calculated using the following equation (Park et al. 2001; Ohko et al. 2001; Yuan and Tsujikawa 1995; Li et al. 2005; Subasri et al. 2006):

$$R = \frac{(W_o - W)}{A \times t} \tag{1}$$

where W_o and W are the weight of the sample before and after immersion in the HCl solution, respectively. A is the surface area of the sample and t is the immersion time.

The inhibition efficiency (%P) of TiO$_2$NTs at different temperatures and time were calculated using the following equation:
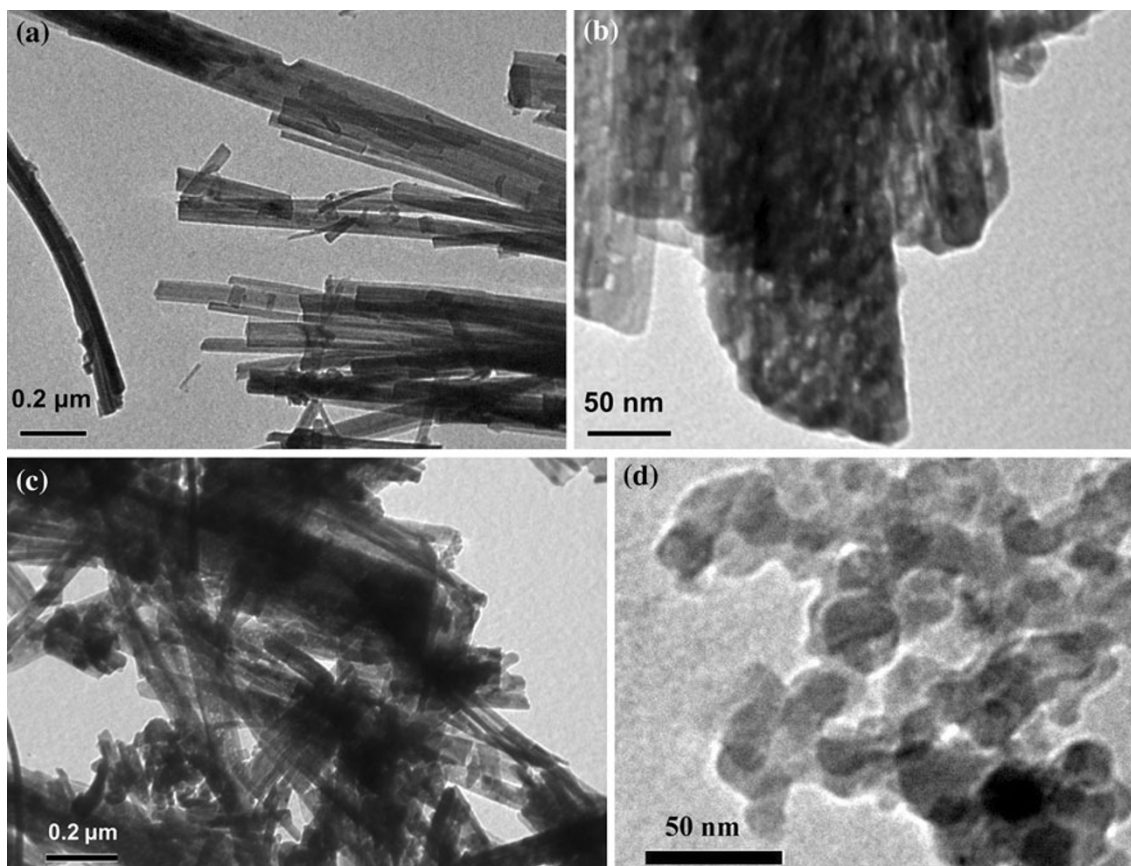

Fig. 1 TEM images of **a** empty anatase TiO$_2$NTs, **b** anatase TiO$_2$NTs filled with NiFe$_2$O$_4$ QDs, **c** anatase TiO$_2$NTs filled with Ni–Fe nanoalloy, and **d** NiFe$_2$O$_4$

$$\%P = 100 \times \left(1 - \frac{W}{W_o}\right) \qquad (2)$$

where $\%P$ is the inhibition efficiency, W_o and W are the weight-loss per min in the HCl solution, respectively.

Magnetic and electrical measurements

The magnetic properties of anatase TiO_2NTs filled with $NiFe_2O_4$ QDs and anatase TiO_2NTs filled with Ni–Fe were investigated using a Vibrating Sample Magnetometer model 9600.

To study electrical conductivity-temperature dependence, compact disks of the samples including empty anatase TiO_2NTs, anatase TiO_2NTs filled with $NiFe_2O_4$ QDs, anatase TiO_2NTs filled with Ni–Fe nanoalloy and $NiFe_2O_4$ were treated at 85 °C for 1 h. The compressed disks were then placed between two stainless steel electrodes in an electrical cell and held tightly with springs. The electrical conductivity cell was made of two ceramic circular bases joined together by four stainless steel rods. The total resistance, R, of the disks was measured directly using a computerized Avometer within the temperature range of 25–850 °C, in air. The data is converted into electrical conductivity using the following equation (Patrakeev et al. 2001, 2004; Patrakeeva et al. 2005):
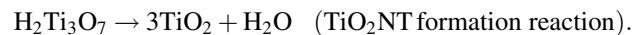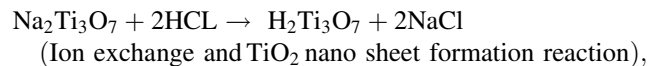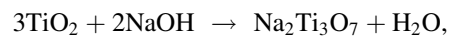
$$S = \frac{l}{A \times R} \qquad (3)$$

where l is the length, A is the cross-sectional area and R is the resistance.

Results and discussion

TiO$_2$NT growth

The mechanism of TiO_2NTs was described in details elsewhere (Farghali et al. 2012) where TiO_2 powder was initially dissolved and hydrolyzed into titanate under the hydrothermal reaction. During the alkali-hydrothermal reaction, the individual monomer of the crystalline precursor can be represented as the $[Ti(OH)_6]^{2-}$ octahedral (Bela et al. 2010). The unstable monomers react via oxolation/olation to form sodium titanate and water. Subsequently, the sodium titanate nanosheets are washed with HCl to form hydrogen titanate and by-product sodium chloride. The Na^+ cations of the octahedra titanium complexes can be substituted with H_3O^+ cations by ion exchange when immersed in HCl for a sufficient time for complete conversion (Wei et al. 2004). Anatase titania can then be obtained under heat treatment dehydration process

of 500 °C. The entire chemical processes that take place could be as follows (Bela et al. 2010):

$$3TiO_2 + 2NaOH \rightarrow Na_2Ti_3O_7 + H_2O,$$

$$Na_2Ti_3O_7 + 2HCL \rightarrow H_2Ti_3O_7 + 2NaCl$$
  (Ion exchange and TiO_2 nano sheet formation reaction),

$$H_2Ti_3O_7 \rightarrow 3TiO_2 + H_2O \quad (TiO_2NT \text{ formation reaction}).$$

Corrosion resistance behavior

TiO_2NTs were tested as coating material for the corrosion protection of Ni–Fe nanoalloy in a corrosive environment. The weight loss of Ni–Fe nanoalloys in a 0.5 M HCl solution with and without TiO_2NTs coatings was plotted as a function of immersion time at different temperatures (25, 50 and 75 °C) as shown in Fig. 2. It shows that the weight loss of uncoated Ni–Fe nanoalloy in 0.5 M HCl solution increases with the immersion time and temperature. Table 1 lists the weight loss of uncoated and coated nanoalloy at different temperatures after an immersion time of 150 min. For TiO_2NTs coated materials the obtained weight loss was found to be very small as compared to uncoated Ni–Fe alloy. It was found that the weight loss of the coated alloys was 21, 27 and 1.5 times less than that of the uncoated alloys at 25, 50 and 75 °C, respectively. It appears also that TiO_2NTs retain their protective ability even after long immersion times.

Figure 2 shows the corrosion rates represented by slope of each curve, mg cm^{-2} min^{-1}, of free Ni–Fe nanoalloy and Ni–Fe coated with TiO_2NTs in 0.5 M HCl. It shows that the corrosion rate of free Ni–Fe nanoalloy increases with increasing the immersion time and temperatures under the prevailing conditions. While in the case of TiO_2NTs coating the corrosion rate was drastically suppressed, the slope was zero at 25 and 50 °C as shown in Fig. 2a, b, respectively. The corrosion rate of the coated alloy slightly increased at 75 °C between an immersion time of 100 and 120 min and retained its stability after that as shown in Fig. 2c. These results indicate that TiO_2NTs could significantly depress the acid interactions with Ni–Fe nanoalloy. Thus, TiO_2NTs could be a good corrosion inhibitor with high protective capability.

Figure 3 shows the variation of the inhibition efficiency ($\%P$) with time at different temperatures. Inhibition efficiency values were 99.3, 99.2 and 87.7 % at 25, 50 and 75 °C, respectively. This indicates that the TiO_2NTs offer high inhibition efficiency even after long immersion time and at high temperatures. This could be attributed to the ceramic protective barrier formed by TiO_2NTs which protects the Ni–Fe nanoalloy from direct contact with the corrosive medium. Furthermore, photo-generated cathodic protection currents increase due to the presence of Ni–Fe nanoalloy inside TiO_2NTs. The Ni–Fe nanoalloy narrows
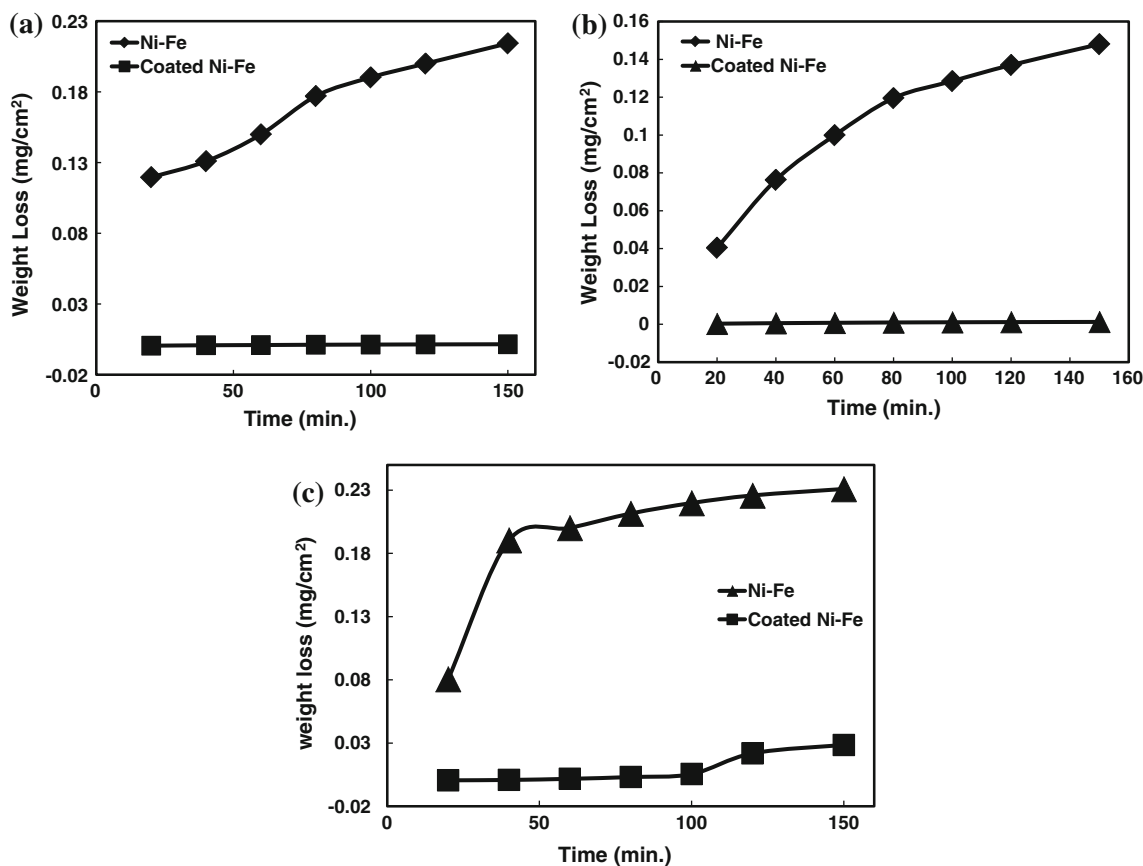
Fig. 2 Corrosion rate of free Ni–Fe nanoalloy and Ni–Fe coated with TiO$_2$NTs in 0.5 M HCl at **a** 25, **b** 50 and **c** 75 °C

Table 1 Weight loss of free and coated Ni–Fe nanoalloy at different temperatures after an immersion time of 150 min

Temperature (°C)	Weight loss (%)	
	Free nanoalloy	Coated nanoalloy
25	63.6	3.1
50	94.5	3.5
75	96.5	62.6

the band gap of TiO$_2$NTs and hence shifts its response to visible region and reduces the potential required for generation of charge carriers. The decrease of inhibition efficiency at a higher reaction temperature (75 °C) could be attributed to diffusion of HCl into TiO$_2$NTs which leads to dissolution of the Ni–Fe nanoalloy. As a result, TiO$_2$NTs offer promising and efficient corrosion inhibitor.

Magnetic properties

Figure 4 shows the variation of magnetization applying a magnetic field of 10 kOe at 25 °C for empty anatase TiO$_2$NTs, anatase TiO$_2$NTs filled with NiFe$_2$O$_4$ QDs and anatase TiO$_2$NTs filled with Ni–Fe alloy. Absence of
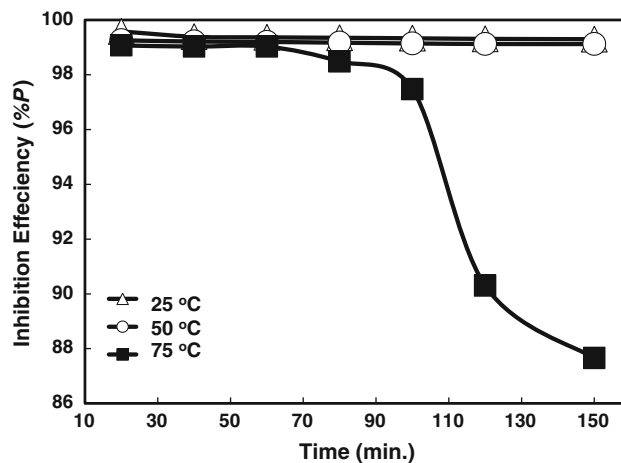

Fig. 3 Inhibition efficiency (P) % of TiO$_2$NTs using weight loss data at temperatures of **a** 25, **b** 50, and **c** 75 °C

hysteresis with very small values of coercivity and remanence near magnetic field of 10 kOe was observed. This could be attributed to the presence of the non-magnetic TiO$_2$ layer on the surface of NiFe$_2$O$_4$. In other words, NiFe$_2$O$_4$ QDs and Ni–Fe nanoalloy are highly distributed in the cavity of TiO$_2$NTs and so the volume of the
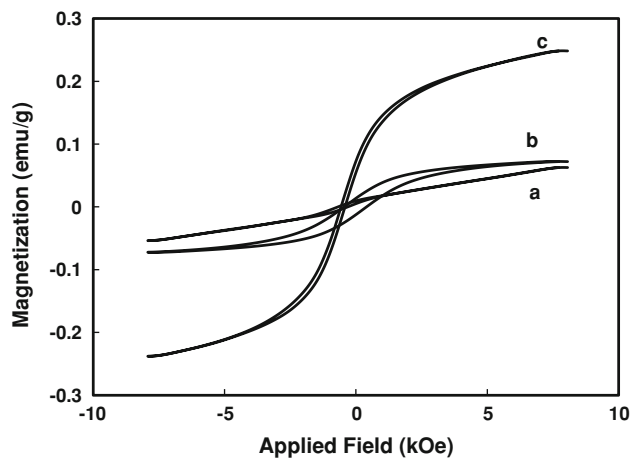
Fig. 4 Variation of magnetization with the applied field at room temperature of **a** empty anatase TiO_2NTs, **b** anatase TiO_2NTs filled with $NiFe_2O_4$ QDs, and **c** anatase TiO_2NTs filled with Ni–Fe nanoalloy

non-magnetic coating layer contributes to the total sample volume. This non-magnetic coating layer acts as a magnetic dead layer on the surface which quenches the magnetic moments affecting magnetization (Zhaoyue et al. 2003; Subasri and Shinohara 2003).

Table 2 shows the values of saturated magnetization (B_s), remnant magnetization (B_r) and coercive force (H_c). It shows that B_s values of TiO_2NTs filled with Ni–Fe nanoalloy are slightly higher than empty TiO_2NTs and TiO_2NTs filled with $NiFe_2O_4$ QDs. This might be due to the magnetic properties of metals are higher than that of oxides. The B_r values for empty TiO_2NTs and TiO_2NTs filled with Ni–Fe nanoalloy are about the same and higher than that of TiO_2NTs filled with $NiFe_2O_4$ QDs.

The non-saturation of the magnetic hysteresis loop and the absence of hysteresis and coercivity at the applied magnetic field indicate the super-paramagnetic nature of the anatase TiO_2NTs coated $NiFe_2O_4$ QDs and Ni–Fe nanoalloy. Thus, the magnetic response of the core is not significantly altered and that the core can still be used to facilitate the removal of composite nanoparticles.

Electrical conductivity

The conductivity-temperature dependence of empty anatase TiO_2, anatase TiO_2NTs filled with $NiFe_2O_4$ QDs,

anatase TiO_2NTs filled with Ni–Fe nanoalloy and $NiFe_2O_4$ compact disks was investigated in the temperature range of 25–850 °C in air. The measurements were carried out in an open vertical furnace under a nearly constant heating and cooling rates of 5 °C/min. Due to moisture and/or gas surface adsorption, the conductivity of the samples showed an unstable and relatively poor initial values at temperatures near 25 °C. At higher temperatures the conductivity increased with temperature due to the semiconductor nature of the samples.

Figure 5 correlates the DC conductivity (σ) of the samples to the temperature during a heating–cooling cycle. During cooling the conductivity retains values higher than that obtained during heating; this may be explained by the fact that the electrical conductivity of semiconductor materials is significantly affected by the oxygen vacancies and/or lattice defects within the sample (Patrakeev et al. 2001, 2004; Patrakeeva et al. 2005).

For empty anatase TiO_2NTs new phases of Ti oxides appeared as a result of heating in air as shown by XRD patterns in Fig. 6. Every phase has its own conductivity mechanism, and the transformation of TiO_2NTs from tubular form to nanorods then nanoparticles will take place at higher temperatures (Zhang et al. 2007), decreasing available conductive samples. Thus, there should be changes in the oxygen vacancies and the number of defects with in crystal lattice and hence the conductivity (Khader et al. 1993). In other words, the oxygen absorption/ desorption into/from the sample that affects the oxygen stoichiometry, and hence the conductivity, is the reason for the observed irreversible conductivity values of the TiO_2NTs during heating–cooling measurements.

The DC conductivity of TiO_2NTs filled with $NiFe_2O_4$ QDs is illustrated in Fig. 5b. During cooling, the samples exhibit reversible behavior. At higher temperatures, the behavior is irreversible due to the phase transformation and destruction of TiO_2NTs. The overall behavior is linear-like which may be attributed to filling $NiFe_2O_4$ with QDs.

Table 3 illustrates the conductivity values [σ (Ωcm)$^{-1}$] of the tested samples at 850 °C. It was found that the conductivity values of empty anatase TiO_2NTs is higher than that of TiO_2NTs filled with $NiFe_2O_4$ QDs. This could be a result of the firing step of TiO_2NTs at 600 °C to form $NiFe_2O_4$ DQs which might affect the defect density and hence the conductivity value.

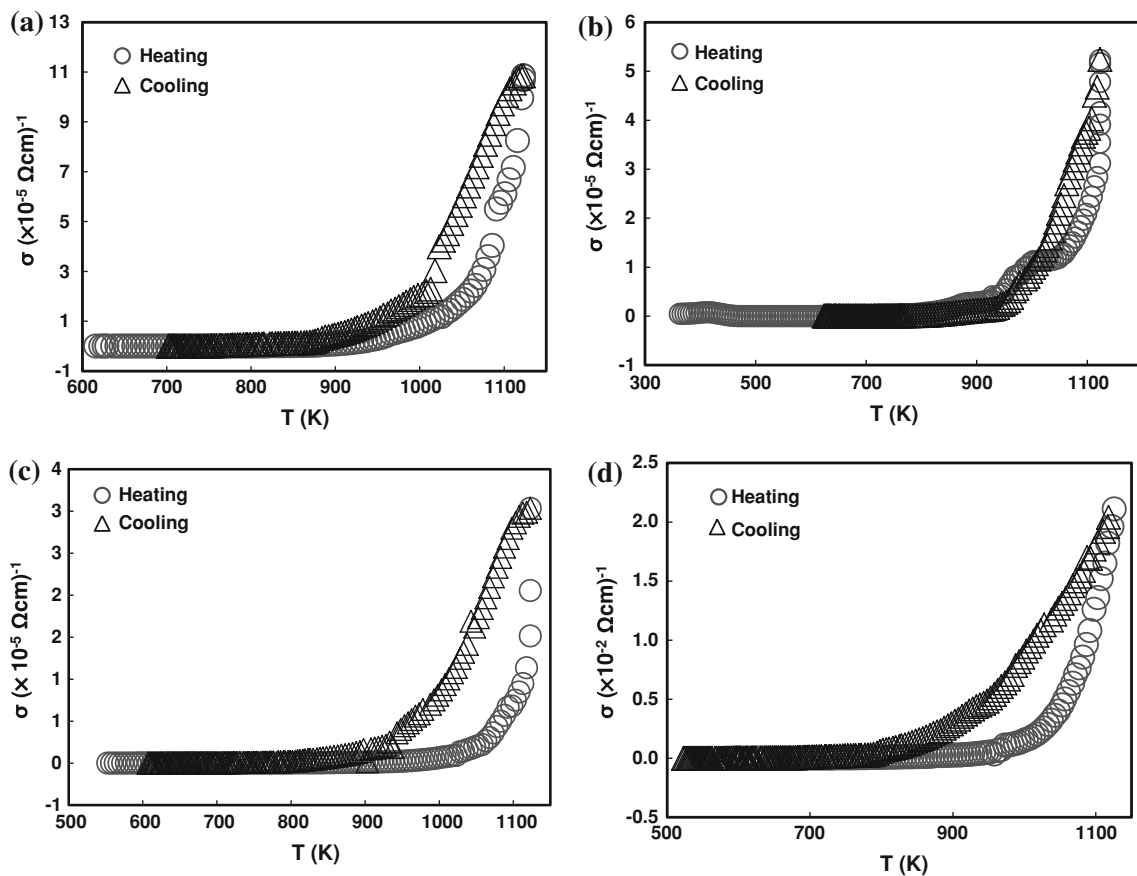|	Saturated magnetization, B_s (emu/g)	Remnant magnetization, B_r (emu/g)	Coercive force, H_c (Oe)
Table 2 Magnetic properties applying magnetic field of 10 KOe at 25 °C			
Empty anatase TiO_2NTs	0.0620	0.0030	193
Anatase TiO_2NTs filled with $NiFe_2O_4$	0.0749	0.0164	364.8
TiO_2NTs filled with Ni–Fe nanoalloy	0.2492	0.0154	59.05

Fig. 5 The conductivity of **a** empty phase TiO$_2$NTs, **b** anatase TiO$_2$NTs filled with NiFe$_2$O$_4$ QDs, **c** anatase TiO$_2$NTs filled with Ni–Fe nanoalloy, **d** NiFe$_2$O$_4$ as a function of temperature during heating–cooling cycle in air
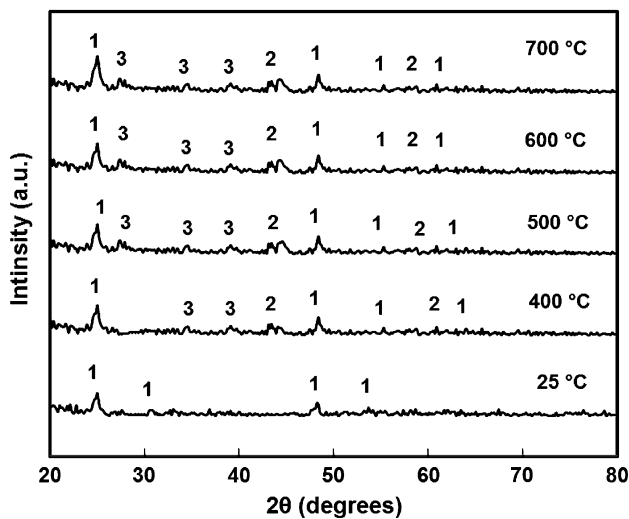

Fig. 6 XRD Patterns under heating of anatase TiO$_2$NTs. Peaks are marked with *numbers 1, 2 and 3* representing anatase TiO$_2$, TiO$_{0.997}$ and rutile-phase TiO$_2$, respectively

Table 3 Conductivity values at 850 °C

Sample	Conductivity $\sigma(\Omega cm)^{-1}$
Empty anatase TiO$_2$NTs	1.0841×10^{-4}
Anatase TiO$_2$NTs filled with NiFe$_2$O$_4$ QDs	5.2385×10^{-5}
Anatase TiO$_2$NTs filled with Ni–Fe nanoalloy	3.0332×10^{-5}
NiFe$_2$O$_4$	0.0204

850 °C are lower than those observed for empty TiO$_2$NTs or TiO$_2$NTs filled with NiFe$_2$O$_4$ QDs. This may be attributed to the reduction process carried out to produce TiO$_2$NTs filled with Ni–Fe nanoalloy. This reduction is believed to affect the density of defects and the oxygen vacancies within the sample as the removal of the adsorbed and structural oxygen from TiO$_2$NTs and NiFe$_2$O$_4$ affects the oxygen stoichiometry and consequently the conductivity of the sample.

For NiFe$_2$O$_4$ the DC conductivity-temperature dependence during a heating–cooling cycle is shown in Fig. 5d. The overall behavior is irreversible during cooling, and shows conductivity values higher than those obtained during heating due to permanent changes in the oxygen

Figure 5c shows the electrical conductivity-temperature dependence of TiO$_2$NTs filled with Ni–Fe nanoalloy. The overall behavior is irreversible. The conductivity values at

vacancies and/or lattice defects within the semiconductor sample. In addition, the $NiFe_2O_4$ conductivity at 850 °C is higher than that of the other three materials. This could be due to the fact that the conduction in ferrite crystals at higher temperature is dominated by ionic hopping mechanism, while at lower temperature, it is due to electronic transfer (Patrakeev et al. 2001, 2004; Patrakeeva et al. 2005).

Furthermore, $NiFe_2O_4$ is a ferromagnetic material with a curie transition temperature around 615–650 °C. The material is transformed from the lower temperature ferromagnetic phase, where electronic conduction dominates the carrier transportation mechanism, to a higher temperature paramagnetic phase, where ions become more mobile and ionic conduction with higher activation energy dominates the carrier transportation mechanism. This transition changes not only the carrier density due to vacancy generation but also the carrier mobility due to increases in lattice defects and phonon scattering.

Conclusions

TiO_2NTs was tested as a corrosion resistant coating for Ni–Fe nanoalloy in 0.5 M HCl solution at 25, 50 and 75 °C and for immersion time of 20, 40, 60 and 150 min. It was found that the weight loss of the coated alloys was 21, 27 and 1.5 times less than that of the uncoated alloys at 25, 50 and 75 °C, respectively. The inhibition efficiency was 99.3, 99.2 and 87.7 % at 25, 50 and 75 °C, respectively showing that TiO_2NTs should be a promising and efficient corrosion inhibitor under the investigated conditions.

The presence of the TiO_2 layer which is non-magnetic on the surface of $NiFe_2O_4$ QDs or Ni–Fe nanoalloy acts as a magnetic dead layer depressing their magnetization values compared to the free form of $NiFe_2O_4$ Ni–Fe nanoalloy.

The electrical conductivity-temperature dependence of empty anatase TiO_2NTs, anatase TiO_2NTs filled with $NiFe_2O_4$ QDs, anatase TiO_2NTs filled with Ni–Fe nanoalloy and $NiFe_2O_4$ compact disks were measured in the temperature 25–850 °C in air.

Empty anatase TiO_2NTs, anatase TiO_2NTs filled with Ni–Fe nanoalloy and $NiFe_2O_4$ showed irreversible behavior, because conduction in semiconductor materials is significantly affected by the oxygen vacancies and/or lattice defects within the sample.

References

Bahgat M, Paek M-K, Pak J-J (2007) Reduction kinetics and mechanisms of $NiFe_2O_4$ with synthesis of nanocrystalline Fe-Ni alloy. Mat Trans 48:3132–3139

Bela S, Wong ASW, Ho GW (2010) Hydrolysis and ion exchange of titania nanoparticles towards large-scale titania and titanate-nanobelts for gas sensing applications. J Phys D Appl Phys 43:035401

Deguchi T, Miyasaki D, Masuhara K, Iwasaki M, Tada H, Ito S, Kyokaishi S (2001) Photocatalytically active nanocomposite films consisting of TiO_2 particles and Zn-Ni alloy electrodeposited on steel plates. J Japan SocColo Mate 74:437–443

Farghali AA, Khedr MH, Moustafa AF (2008) Photocatalytic activity and magnetic properties of nanocrystallite strontium hexaferrite prepared by self-flash combustion. J Mater Techno 23:104–109

Farghali AA, Bahgat A, Moustafa AF, Khedr MH (2012) Synthesis and characterization of TiO_2 nanotubes filled with $NiFe_2O_4$ quantum dots. Submitted

Fathi AA (2011) Synthesis and charecterization of TiO_2 nanotubes (TiO_2NTs) filled with highly efficient quantum dots. Dissertation, Beni-Suef University

Hong Y, Jing L, Hong-Bo C, Chang-Jian L (2007) A study on the N-, S- and Cl-modified nano-TiO_2 coatings for corrosion protection of stainless steel. J Electrochimica Acta 52:6679–6685

Jin Y, Yong-kang L, Yu L, Jun-ping L (2010) Synthesis and characterization of magnetic $TiO_2/SiO_2/NiFe_2O_4$ composite photocatalysts. J Chem Res Chin Univ 26:278–282

Khader MM, Kheiri FMN, El-Anadouli BE, Ateya BG (1993) Mechanism of reduction of rutile with hydrogen. J Phys Chem 97:6074–6077

Lee JS, Kim TH, Yu JH, Chung SW (1997) In situ alloying on synthesis of nanosized Ni-Fe powder. Nanostruct Mater 9:153–156

Li J, Jing J, He H, Sun Y (2002) Synthesis, microstructure, and mechanical properties of TiO_2/Ni nanocomposite coatings. J Mater Sci Lett 21:939–941

Li M, Luo SZ, Wu PF (2005) Photocathodic protection effect of TiO_2 films for carbon steel in 3% NaCl solutions. J Electrochim Acta 50:3401–3406

Lunhong A, Jing J (2009) An investigation on synthesis and magnetic properties of ferromagnetic nanoparticles of nickel ferrite coated with TiO_2. J Mater Sci Mater Electron 20:257–261

Meinert K, Uerpmann C, Matschullat J, Wolf GK (1998) Corrosion and leaching of silver doped ceramic IBAD coatings on SS 316L under simulated physiological conditions. Surf Coat Technol 58:103–104

Millot M, Blanchin G, Tetot R, Marucco JF, Poumellec B, Picard C, Touzlin B (1987) High temperature nonstoichiometric rutile TiO_{2-x}. J Solid State Chem 17:263–293

Ohko Y, Saitoh S, Tatsuma S, Fujishima A (2001) Photoelectrochemical anticorrosion and self-cleaning effects of a TiO_2 coating for type 304 stainless steel. J Electrochem Soc 148:24–28

Park H, Kim KY, Choi W (2001) A novel photoelectrochemical method of metal corrosion prevention using a TiO2 solar panel. Chem Comm 1:281–282

Patrakeev MV, Mitberg EB, Leonidov IA, Kozhevnikov VL (2001) Electrical characterization of the intergrowth ferrite $Sr_4Fe_6O_{13+\delta}$. J Solid State Ion 139:325–330

Patrakeev MV, Leonidov IA, Kozhevnikov VL, Kharton VV (2004) Ion–electron transport in strontium ferrites: relationships with structural features and stability. J Sol State Sci 6:907–913

Patrakeeva MV, Leonidova IA, Kozhevnikova VL, Poeppelmeier KR (2005) p-Type electron transport in $La_{1-x}Sr_xFeO_{3-\delta}$ at high temperatures. J Sol State Chem 178:921–927

Peng CH, Hwang CC, Wan J, Tsai JS, Chen SY (2005) Microwave-absorbing characteristics for the composites of thermal-plastic polyurethane (TPU)-bonded NiZn-ferrites prepared by combustion synthesis method. Mater Sci Eng B 117:27–36

Praveen BM, Venkatesha TV (2008) Electrodeposition and properties of Zn-nanosized TiO_2 composite coatings Electrodeposition and properties of Zn-nanosized TiO_2 composite coatings. App Surf Sci 254:2418–2424

Radhakrishnana S, Siju CR, Debajyoti M, Satish P, Giridhar M (2009) Conducting polyaniline–nano-TiO_2 composites for smart corrosion resistant coatings. J Electrochimica Acta 54:1249–1254

Rana R, Srivastava S, Sorensson MM, Misra RDK (2005) Synthesis and characterization of nanoparticles with magnetic core and photocatalytic shell: anatase TiO_2–$NiFe_2O_4$ system. Mater Sci Eng B 119:144–151

Sang OC, Didier K, Filofteia LT, Ghislaine B, Hanlin L, Christian C, Akira O (2005) Microstructure and mechanical properties of plasma sprayed nanostructured TiO_2–Al composite coatings. J Surface & Coatings Technology 194:215–224

Seshamma NV, Chandra S, Ravinder D (2006) Thermoelectric power studies of La^{3+} substituted strontium hexagonal ferrites. J Alloys Comp 421:1–3

Shen GX, Chen YC, Lin CJ (2005) Corrosion protection of 316 L stainless steel by a TiO_2 nanoparticle coating prepared by sol–gel method. Thin Solid Films 489:130–136

Shinohara T (2001) Impedance measurement for slow decline of electrode potential of Fe-doped TiO_2 coatings. Corros Eng 50:170–176

Shiyan Z, Qing L, Xiaokui Y, Xiankang Z, Yan D, Fei L (2010) Corrosion resistance of AZ91D magnesium alloy with electroless plating pretreatment and Ni–TiO_2 composite coating. J Mater Charact 1:269–276

Sorensen OT (1981) Nonstoichiometric oxides. Academic Press, New York

Subasri R, Shinohara T (2003) Investigations on SnO_2–TiO_2 composite photoelectrodes for corrosion protection. J Electrochem Commun 5:897–902

Subasri R, Deshpande S, Seal S, Shinohara T (2006) Evaluation of the performance of TiO_2–CeO_2 bilayer coatings as photoanodes for corrosion protection of copper electrochem. J Electrochem Solid State Lett 9:1–4

Tatsuma T, Satioh S, Ohko Y, Fujishima (2001) TiO_2–WO_3 Photoelectrochemical anticorrosion system with an energy storage ability. J Chem Mater 13:2838–2842

Tatsuma T, Saitoh S, Ngaotrakanwiwat P, Ohko Y, Fujishima (2002) Energy storage of TiO_2–WO_3 photocatalysis systems in the gas phase. Langmuir 18:7777–7779

Vinodgopal K, Bedja I, Kamat PV (1996) Nanostructured semiconductor films for photocatalysis: photoelectrochemical behavior of SnO_2/TiO_2 composite systems and its role in photocatalytic degradation of a textile azo dye. Chem Mater 8:2180–2187

Wei M, Konishi Y, Zhou H, Sugihara H, Arakawa H (2004) A simple method to synthesize nanowires titanium dioxide from layered titanate particles. Chem Phys Lett 400:231–234

Xiao HM, Liu XM, Fu SY (2006) Synthesis, magnetic and microwave absorbing properties of core-shell structured $MnFe_2O_4$/TiO_2 nanocomposites. JCST 66:2003–2008

Yuan J, Tsujikawa S (1995) Characterization of sol–gel-derived TiO2 coatings and their photoeffects on copper substrates. J Electrochem Soc 142:3444–3450

Zainullina VM, Korotin MA, Kozhevnikov VL (2006) Electronic structure and properties of strontium ferrite $Sr_3Fe_2O_6$. Eur Phys J B 49:425–431

Zhang L, Lin H, Wang N, Lin C, Li J (2007) The evolution of morphology and crystal form of titanate nanotubes under calcination and its mechanism. J Alloy Compo 424:230–235

Zhaoyue L, Pan K, Meijia W, Min L, Qiang L, Yubai B, Teijin L (2003) Influence of the mixed ratio on the photocurrent of the TiO_2/SnO_2 composite photoelectrodes sensitized by mercurochrome. J Photochem Photobiol A Chem 157:39–46